Retention of the Radiotracers ^{64}Cu-ATSM and ^{64}Cu-PTSM in Human and Murine Tumors Is Influenced by MDR1 Protein Expression

Jun Liu[1,2], Asghar Hajibeigi[1], Gang Ren[1], Mai Lin[1], Wasana Siyambalapitiyage[1], Zhisu Liu[2], Evan Simpson[3], Robert W. Parkey[1], Xiankai Sun[1], and Orhan K. Öz[1]

[1]*Department of Radiology, UT Southwestern Medical Center at Dallas, Dallas, Texas;* [2]*Department of Surgery, Zhongnan Hospital of Wuhan University, Wuhan University, Wuhan, China; and* [3]*Prince Henry's Institute of Medical Research, Clayton Vic, Australia*

Tumor hypoxia is often associated with resistance to chemotherapy. Multidrug resistance type 1 (MDR1) protein is a member of the adenosine triphosphate binding cassette (ABC) proteins, some of which are involved in the multidrug resistance (MDR) phenotype in tumors. Many studies have focused on the role of these proteins in modulating drug resistance, but their effect on retention of imaging agents is less well studied. To study the role of MDR1 expression on the accumulation of ^{64}Cu-diacetyl-bis(*N*4-methylthiosemicarbazone) (^{64}Cu-ATSM) and ^{64}Cu-pyruvaldehyde-bis(*N*4-methylthiosemicarbazone) (^{64}Cu-PTSM) in human tumors in vitro and in vivo, we used a model system composed of a low MDR1–expressing parent uterine sarcoma cell line and a daughter cell line selected for overexpression of MDR1. Aromatase knockout (ArKO) mice that spontaneously developed liver tumors were used as an additional in vivo model to study the effect of MDR expression on ^{64}Cu-ATSM and -PTSM retention. **Methods:** Biodistribution experiments after injection of ^{64}Cu-ATSM or -PTSM were performed in wild-type mice, ArKO mice, and ArKO mice bearing liver tumors (n = 3–5/group), and in nude mice bearing human tumor xenografts for in vivo PET/CT. Liver expression of *Abcb1a* and *Abcb1b*, the MDR1 proteins in mouse liver, was determined by real-time polymerase chain reaction. ^{64}Cu-ATSM and -PTSM accumulation and efflux studies were conducted in tumor cell lines. The uptake experiments were repeated after knockdown of MDR1 protein expression using MDR1-specific small interfering RNAs. **Results:** In vivo, the hepatic tumors had a lower percentage injected dose per gram of ^{64}Cu-ATSM or -PTSM and more highly expressed *Abcb1b* than did wild-type liver or nontumor-bearing ArKO liver. High MDR1–expressing tumors showed lower tracer activity on PET/CT images. In vitro, cells highly expressing MDR1 had significantly decreased ^{64}Cu-ATSM and -PTSM retention and enhanced efflux. Knockdown of MDR1 expression significantly enhanced the ^{64}Cu-ATSM and -PTSM retention and decreased the efflux in MDR1-positive cells. **Conclusion:** The expression of MDR1 glycoprotein (or its equivalents in mice) affects the retention of ^{64}Cu-ATSM and -PTSM in the human and murine tumors tested. These results may have implications for clinical hypoxia imaging in tumors and the therapeutic efficacy of ^{64}Cu-ATSM.

Key Words: MDR1; P-glycoprotein (Pgp); hypoxia imaging; copper-diacetyl-bis(*N*4-methylthiosemicarbazone); copper-pyruvaldehyde-bis(*N*4-methylthiosemicarbazone)

J Nucl Med 2009; 50:1332–1339
DOI: 10.2967/jnumed.109.061879

Tumor hypoxia has been implicated in the development of resistance to chemoradiation therapy and increased metastatic potential (*1*). Resistance to individual cytotoxic drugs can occur, but it can also occur more broadly to a variety of drugs with different chemical structures and different mechanisms of action. The latter form of resistance is called multidrug resistance, or MDR (*2*). One of the cellular mechanisms of MDR involves a 170-kDa glycoprotein MDR1 (ABCB1/P-glycoprotein), an adenosine triphosphate (ATP)–dependent efflux pump for several anticancer agents (*3*). MDR1, a member of the ATP-binding cassette (ABC) superfamily of membrane transport proteins, recognizes and acts on several clinically important chemotherapeutic compounds including taxanes, etoposides, and Vinca alkaloids (*2*). Although the mechanisms of MDR1 function and modulation are incompletely understood, studies have shown a strong link between the level of MDR1 expression and treatment outcome; cells with higher levels of MDR1 expression have poorer responses and are more likely to become refractory (*2*).

The importance of predicting resistance to therapy has resulted in an intense effort to noninvasively assess tumor hypoxia. Molecular imaging potentially affords noninvasive methods to assess tumor hypoxia and thereby potentially predict response to or direct timing of therapy. The most widely known imaging agent that is an MDR1 substrate is the lipophilic cationic radiopharmaceutical ^{99m}Tc-hexakis-

Received Jan. 6, 2009; revision accepted Apr. 29, 2009.
For correspondence or reprints contact: Orhan K. Öz, Department of Radiology, UT Southwestern Medical Center at Dallas, 5323 Harry Hines Blvd., Dallas, TX 75390-9153.
E-mail: Orhan.Oz@UTSouthwestern.edu

2-methoxyisobutylisonitrile (^{99m}Tc-MIBI) (*4*). In general, studies have shown that tumor cells with high MDR1 expression show lower accumulation and faster washout of the tracer than do their parental cells with lower MDR1 expression (*5–10*). A few studies have found decreased tumor or tumor cell retention of ^{99m}Tc-MIBI in the presence of lower oxygen tension (*7–9*). ^{99m}Tc-MIBI is used for conventional planar imaging or SPECT. Because PET has intrinsic advantages over SPECT in terms of quantification, tracers have been developed for PET of hypoxia.

Nitroimidazole compounds are metabolically trapped in tissues with low oxygen tensions. ^{18}F-fluoromisonidazole (^{18}F-FMISO) is the most widely studied nitroimidazole for in vivo PET (*11*). Unfortunately, ^{18}F-FMISO has low tissue uptake, resulting in limited tumor-to-blood contrast and slow cellular release. These factors delay imaging and limit image quality (*12*). Copper bis(thiosemicarbazone) complexes have been developed for PET hypoxia imaging and perfusion. The dithiosemicarbazones were first shown 40 y ago to have greater antitumor effects when complexed with Cu(II) (*13*). ^{64}Cu-pyruvaldehyde-bis(*N*4-methylthiosemicarbazone) (^{64}Cu-PTSM), which lacks hypoxia selectivity, is a PET perfusion tracer with distribution proportional to the blood flow. ^{64}Cu-diacetyl-bis(*N*4-methylthiosemicarbazone) (^{64}Cu-ATSM) differs in only 1 methyl group from PTSM and possesses a lower redox potential; consequently, ^{64}Cu-ATSM is more readily reduced and trapped in hypoxic tissues. ^{64}Cu-ATSM overcomes some of the limitations of FMISO in that it shows rapid tumor delineation and high tumor-to-blood ratios (*12*). The first demonstration of the hypoxia selectivity of ^{64}Cu-ATSM was in an isolated rat heart model of ischemia (*14*). Subsequently, ^{64}Cu-ATSM has been shown to be predictive of radiotherapy treatment outcome in small clinical trials (*15,16*). However, some studies have shown tumor type–dependent hypoxia selectivity of ^{64}Cu-ATSM, and factors other than hypoxia may contribute to the tumor retention of this radiotracer (*17–19*).

With these considerations in mind, we designed studies to determine whether, like ^{99m}Tc-MIBI, ^{64}Cu-ATSM and -PTSM may be substrates for the MDR1. ^{64}Cu-ATSM and -PTSM retention was compared in an MDR1(−) parent tumor cell line and in an MDR1(+) overexpressing cell line, selected from it, both in in vitro and in in vivo xenografts. Further, we tested ^{64}Cu-ATSM and -PTSM liver retention in mice deficient in the enzyme aromatase that develop spontaneous liver tumors.

MATERIALS AND METHODS

Cell Culture

The human uterine sarcoma cell lines MES-SA and MES-SA/Dx5 were purchased from the American Type Culture Collection (ATCC; CRL-1976 and CRL-1977). MES-SA/Dx5 is an MDR cell line selected from MES-SA (*20*). The cell lines were grown in ATCC-formulated McCoy's 5a medium, modified (catalog no. 30-2007; ATCC), supplemented with 10% fetal bovine serum.

Animals

All procedures were approved by the UT Southwestern Institutional Animal Care and Use Committee. Generation of aromatase knockout (ArKO) mice has been previously described (*21*). Eighteen- to 20-mo-old male wild-type and ArKO mice of mixed C57BL/6J and 129SvEvTaconic genetic background were maintained in a specific pathogen-free environment with food and water ad libidum. ArKO mice with hepatic tumors were identified by palpation. Male wild-type ($n = 5$), ArKO ($n = 5$), and ArKO mice with liver tumors ($n = 3$) were injected with 0.37 MBq of ^{64}Cu-ATSM or ^{64}Cu-PTSM. After a 1-h uptake period, the livers were harvested, weighed, and counted. Standards were prepared and counted along with the samples to calculate the percentage injected dose per gram of tissue (%ID/g). To establish human tumor xenografts, 10^7 cells/cell line were suspended in 100 μL of culture medium and implanted subcutaneously into 3 athymic nude mice as follows: MES-SA cells were injected about the left shoulder and MES-SA/Dx5 cells were injected about the right shoulder. Mice ($n = 3$) were scanned 22 d after implantation.

Preparation of ^{64}Cu-ATSM and ^{64}Cu-PTSM

All reagents and solvents were purchased from Sigma-Aldrich and used as received. Milli-Q water (18 MΩ·cm) was obtained from a Millipore Gradient Milli-Q water system and used for all radiochemistry procedures and biologic evaluations. Millipore C_{18} Sep-Pak cartridges were pretreated with ethanol and water before use. All reaction vials were acid-washed with 10%−20% nitric acid overnight. Silica gel 60 F_{254} plates were purchased from Merck & Co. ^{64}Cu-chloride (in 0.1N HCl) was purchased from University of Wisconsin at Madison. ^{64}Cu-ATSM and ^{64}Cu-PTSM were produced by the method previously described (*22,23*). The radiochemical purity was greater than 98%, and the specific activity was about 0.15 MBq/μg. Injection doses (~0.37 MBq in 100 μL) were prepared by diluting ^{64}Cu-ATSM or ^{64}Cu-PTSM with saline (ethanol < 5%).

Mouse PET/CT

Small-animal PET/CT studies were performed using a Siemens Inveon PET/CT Multimodality System. Mice were injected with 3.7 MBq (100 μCi) of ^{64}Cu-ATSM via the tail vein. Ten minutes before imaging, the animals were anesthetized using 3% isoflurane at room temperature until stable vitals were established. Once an animal was sedated, it was placed onto the imaging bed under 2% isoflurane anesthesia for the duration of the imaging. The CT data were acquired at 80 kV and 500 μA, with a focal spot of 58 μm. The effective pixel size was 103.03 μm. CT images were reconstructed with a down-sample factor of 2 using reconstruction software (Cobra). PET images, obtained directly after the CT scans, were acquired at 1 h after injection of ^{64}Cu-ATSM for 15 min. PET images were reconstructed using Fourier rebinning and the ordered-subsets expectation maximization 3D algorithm. The reconstructed images were fused and analyzed using the Inveon Research Workplace (IRW) software (Siemens). Liver or tumor regions of interest were selected on serial axial images, and the activity was quantified using the IRW software.

RNA Isolation and Quantitative Real-Time Polymerase Chain Reaction (qRT-PCR)

Total cellular RNA was isolated using an RNeasy kit (Qiagen). To measure MDR1 messenger RNA (mRNA) levels in MES-SA and MES-SA/Dx5 cells, 1 μg of total cellular RNA from each cell line was reverse-transcribed into first-strand cDNA using an

iScriptTM cDNA synthesis kit (Bio-Rad). MDR1 mRNA was quantified by qRT-PCR using the comparative cycle threshold method. All primer sets are listed in Table 1. Twenty-five-microliter reactions were performed in a 96-well plate, using the PCR amplification protocol, 95°C denaturation (3 min), and 40 amplification cycles (95°C for 30 s, 57°C for 30 s, and 72°C for 1 min), in an iCycler iQ real-time thermocycler (Bio-Rad). The 18S ribosomal subunit was used as an internal reference gene. The MES-SA mean MDR1 was used as the calibrator. All experiments were repeated 3 times using triplicates in each experiment. *Abcb1a* and *Abcb1b* mRNA levels in mouse liver or liver tumor samples were also quantified by qRT-PCR using glyceraldehyde-3-phosphate dehydrogenase as an internal reference gene and wild-type liver mean values for each gene as calibrators. Quality control was performed using both electrophoresis analyses on a 2% NuSieve agarose gel (3:1; FMC Bioproducts) and melting curve analysis performed immediately after the end of amplification.

RNA Interference

MDR1 protein expression was suppressed by small interfering RNA (siRNA) duplexes. siRNA for Lamin A/C was used as a control. Control and MDR1-specific duplex siRNAs (Table 1) were purchased from Invitrogen. Twenty-four hours after plating, MES-SA or MES-SA/Dx5 cells were transfected either with 3 siRNA duplexes together (13.3 pmol each) or with control siRNA (40 pmol) using Lipofectamine 2000 reagent (Invitrogen) according to the manufacturer's instructions. Transfection was allowed to proceed for 4 h, after which fresh medium was added. The cells were allowed to grow for 24 h after the transfection, then used for ^{64}Cu-ATSM and -PTSM uptake studies. The experiment was performed twice, with triplicates in each assay.

Western Blot Analysis

Cells were incubated with lysis buffer (50 mM *N*-[2-hydroxyethyl]piperazine-*N*′-[2-ethanesulfonic acid], 150 mM NaCl, 1.5 mM $MgCl_2$, 0.5 mM ethylenediaminetetraacetic acid, 10% glycerol, 1% Triton X-100 (Sigma), 10 mM NaF, 1 mM dithiothreitol, and 1 mM phenylmethylsulfonyl fluoride) for 15 min and then were alternately frozen (−80°C) and thawed 3 times to rupture the cell membranes. Subsequently, the lysates was centrifuged at 12,000*g* for 5 min to pellet the cell membranes or subcellular organelles. The liver was first cut into small pieces, homogenized in lysis buffer using a Dounce homogenizer (Wheaton), and processed in the same manner as cell lysates. Protein concentrations were determined by a standard Bradford assay (Bio-Rad). Equal amounts of protein (20 μg) from each cell line were subjected to Western blot analysis. The antibodies used for probing were mouse anti-MDR (1:1,000; sc-1517 [Santa Cruz Biotechnology, Inc.]) and mouse antiactin (1:5,000; 51K4888 [Sigma]).

Radiotracer Uptake and Efflux Studies

Cell monolayers were washed with phosphate-buffered saline (PBS). Subsequently, serum-free medium containing 3.7 kBq of ^{64}Cu-ATSM or -PTSM per milliliter was added to each well. Cells were incubated with each radiotracer for various times up to 1 h. The uptake was terminated by removal of the medium and rapid washing 3 times with ice-cold PBS. For efflux studies, the cells were loaded with ^{64}Cu-ATSM or -PTSM by placing them in serum-free medium containing 7.4 kBq of ^{64}Cu-ATSM or -PTSM per milliliter for 15 min, followed by an efflux period of up to 2 h in cold medium. The efflux was terminated at the various times by removal of the medium and rapid washing 3 times with ice-cold PBS. All points were performed in triplicate. After the washes, the cells were resuspended in 100 μL of cold lysis buffer, and the radioactivity was measured using a calibrated γ-counter (Perkin Elmer). The ratio of activity per milligram of protein was calculated for each sample and defined as the retained activity. In uptake studies, retained activity was normalized to the MES-SA 1-h value to demonstrate relative accumulation. In efflux studies, time–activity curves for each cell line were generated by normalizing activity to the 15-min value to demonstrate washout.

Statistics

Data are presented as the mean ± SE. The Student *t* test was used to analyze for significant differences between groups. The uptake and efflux data were analyzed by 2-factor ANOVA and

TABLE 1. Primer and siRNA Sequences

Gene	Primer sequence	siRNA duplex sequence
MDR1(ABCB1) forward	5′-TCGTAGGAGTGTCCGTGGAT-3′	
MDR1 (ABCB1) reverse	5′-CATTGGCGAGCCTGGTAG-3′	
Mdr1a (Abcb1a) forward	5′-TACGCCTACTATTACACCG-3′	
Mdr1a (Abcb1a) reverse	5′-CCAGCCTATCTCCTGATT-3′	
Mdr1b (Abcb1b) forward	5′-TCGCTTGTCTACAGTTCG-3′	
Mdr1b (Abcb1b) reverse	5′-GCATTATTTCCTGGTTCA-3′	
18S forward	5′-GGAATTGACGGAAGGGCACCACC-3′	
18S reverse	5′-GTGCAGCCCCGGACATCTAAGG-3′	
GAPDH forward	5′-CTGCCATTTGCAGTGGCAAAGTGG-3′	
GAPDH reverse	5′-TTGTCATGGATGACCTTGGCCAGG-3′	
MDR1 siRNA		5′-GAGUGGGCACAAACCAGAUAAUAUU-3′ 5′-AAUAUUAUCUGGUUUGUGCCCACUC-3′
		5′-CCAUAAAUGUAAGGUUUCUACGGGA-3′ 5′-UCCCGUAGAAACCUUACAUUUAUGG-3′
		5′-GCUCGCCAAUGAUGCUGCUCAAGUU-3′ 5′-AACUUGAGCAGCAUCAUUGGCGAGC-3′
Lamin A/C control siRNA		5′-CUGGACUUCCAGAAGAACAdTdT-3′ 5′-UGUUCUUCUGGAAGUCCAGdTdT-3′

GADPH = glyceraldehyde-3-phosphate dehydrogenase.

post hoc analysis using a *t* test. In all cases, a *P* value of less than 0.05 was considered as statistically significant.

RESULTS

Reduced Accumulation of ^{64}Cu-ATSM and -PTSM In Vivo Correlates with Elevated MDR1 Protein Expression

ArKO mice sporadically develop spontaneous hepatomas (*24*), providing a convenient model to examine ^{64}Cu-ATSM and -PTSM retention in an in vivo system. In biodistribution studies, the %ID/g of ^{64}Cu-PTSM was greatest in the liver of wild-type mice (Fig. 1). The largest difference was between wild-type and ArKO tumor–bearing mice (P = 0.09 for wild-type vs. ArKO and P = 0.04 for wild-type vs. ArKO tumor, Fig. 1A). A similar pattern was observed for ^{64}Cu-ATSM, with wild-type %ID/g being approximately twice that of ArKO tumor–bearing mice (P = 0.08 for wild-type vs. ArKO and P = 0.03 for wild-type vs. ArKO tumor, Fig. 1B). ^{64}Cu-ATSM activity in the liver tumor slices was significantly lower than normal or ArKO liver (Supplemental Fig. 1; supplemental materials are available online only at http://jnm.snmjournals.org). PET/CT images of a wild-type mouse and an ArKO tumor–bearing mouse after ^{64}Cu-ATSM injection clearly show decreased retention in the liver tumor of the ArKO mouse (Figs. 2A and 2B). The decreased liver activity seen on images correlated well with the location of a large hepatic mass. These differences are shown to good advantage in 3D movies (Supplemental Fig. 2).

MDR1 in mice includes Mdr1a and Mdr1b genes. Relative to wild-type, there was about a 2.5-fold increase of Mdr1a mRNA expressions in ArKO liver and ArKO liver tumor (Fig. 3A). The Mdr1b mRNA levels in ArKO liver and ArKO liver tumor were increased by 3.7- and 43-fold, respectively ($P < 0.05$ and < 0.00001 vs. wild-type, Fig. 3B). The MDR1 protein isoforms are recognized as a single 170-kD band on Western blot. In both ArKO liver and ArKO liver tumors, the 170-kD band is clearly greater than in wild-type, with the tumors having highest levels (Fig. 3C and 3D).

Aromatase is a microsomal enzyme and an electron acceptor from the nicotinamide adenine dinucleotide (NADH) cytochrome reductase, one of the enzymes that catalyzes the bioreduction of ^{64}Cu-ATSM. Thus, strictly speaking we cannot exclude the possible contribution of altered microsomal electron transport activity in the ArKO model. To test whether MDR1 expression influences ^{64}Cu-ATSM or -PTSM retention independently of any potential changes in the electron transport system, in vivo PET/CT was performed on mice bearing xenografts of the high MDR1–expressing MES-SA/Dx5 cell line and its nonexpressing parental cell line, MES-SA. PET/CT images acquired 1 h after injection of ^{64}Cu-ATSM clearly revealed significantly decreased retention in the high MDR1–expressing MES-SA/Dx5 cells (Fig. 4). These differences are shown to good advantage in 3D movies (Supplemental Fig. 3).

Knockdown of MDR1 Expression Increases Cellular Retention of ^{64}Cu-ATSM and -PTSM

The MES-SA/Dx5 model was first functionally validated using ^{99m}Tc-MIBI retention as the substrate (Supplemental Fig. 4). Our in vivo studies established an inverse relationship between MDR1 expression and liver retention of ^{64}Cu-ATSM and -PTSM. To test specifically a role for MDR1 in cellular accumulation of ^{64}Cu-ATSM and -PTSM, we reduced MDR1 protein concentration using RNA interference technology. Transfection of MES-SA/Dx5 with siRNA duplexes specific for MDR1 decreased protein levels by 70% (Fig. 5). Uptake and efflux experiments were then performed. Intracellular accumulation of ^{64}Cu-ATSM was lower in MES-SA/Dx5 cells than in MES-SA cells ($P <$ 0.05 at all time points, Fig. 6A). Knockdown of MDR1 in MES-SA/Dx5 cells changed retention such that there was no significant difference in activity between MES-SA– and siRNA-treated MES-SA/Dx5 cells except at 5 min (Fig. 6A). Efflux of ^{64}Cu-ATSM was significantly greater for MES-SA/Dx5 cells (Fig. 6B). Knockdown of MDR1 substantially diminished the efflux rate in MES-SA/Dx5 cells, though not equal to MES-SA cells (e.g., $P < 0.01$ at 45 and 120 min). This result is consistent with other factors also contributing to retention of the radiotracer. Similar patterns of accumulation and efflux were observed between the cell lines for the radiotracer ^{64}Cu-PTSM; however, compared with ^{64}Cu-ATSM assays, there was a greater difference in accumulation between MES-SA and MES-SA/Dx5 and the knockdown was less effective in blunting efflux at the early times (Figs. 6C and 6D).

DISCUSSION

Tumor hypoxia imaging is currently of great clinical interest because of the therapeutic limitations imposed by hypoxia. Hypoxia-induced resistance to chemotherapy asso-

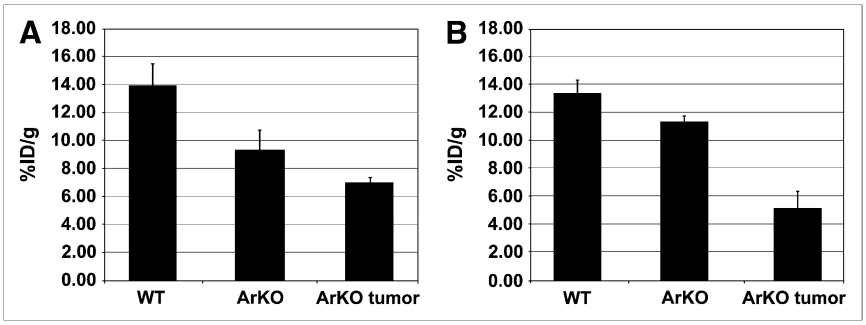

FIGURE 1. Decreased liver retention of ^{64}Cu-ATSM or -PTSM in ArKO and ArKO liver tumor–bearing mice. Male wild-type (n = 5), ArKO (n = 5), and ArKO mice with liver tumors (n = 3) were injected with 3.7 MBq of ^{64}Cu-PTSM (A) or 3.7 MBq of ^{64}Cu-ATSM (B). After 1-h uptake, livers were harvested and weighed, and activity was determined. Results are expressed as mean ± SE.

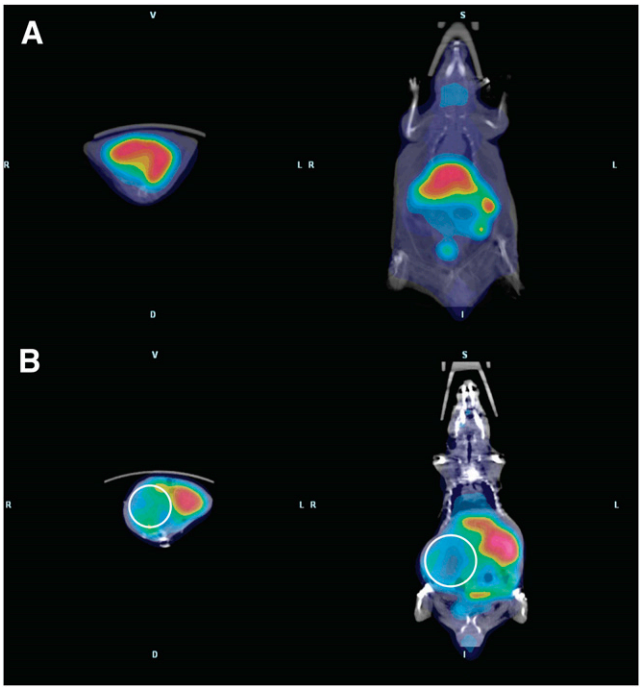

FIGURE 2. PET/CT shows decreased retention of ^{64}Cu-ATSM in ArKO tumor–bearing mice. Whole-body PET/CT images were acquired for wild-type (A) and ArKO tumor–bearing (B) mice 1 h after the intravenous injection of 3.7 MBq (100 μCi) of ^{64}Cu-ATSM. Images show protuberant abdomen in ArKO tumor–bearing mouse and clearly decreased activity in right side of enlarged liver (circles).

ciated with increased MDR1 expression has been known for more than 2 decades (*25*). The relationship between multidrug resistance, hypoxia, and MDR1 activity and expression has been established for several tumor types, although the association may be dependent on the tissue and tumor cell line (*26–28*). To our knowledge, our results show for the first time that, similar to the retention of ^{99m}Tc-MIBI, the cellular and tumoral retentions of both ^{64}Cu-PTSM and ^{64}Cu-ATSM—which have been described as PET perfusion and hypoxia imaging radiotracers, respectively—are influenced by MDR1 protein expression.

Our in vivo studies on both human and mouse models demonstrated an inverse relationship between MDR1 expression and retention of both ^{64}Cu-ATSM and ^{64}Cu-PTSM. The highly MDR1-expressing MES-SA/Dx5 cells showed markedly lower ^{64}Cu-ATSM retention on PET/CT. In biodistribution and imaging studies, liver tumors in ArKO mice demonstrated lower ^{64}Cu-ATSM and -PTSM retention than wild-type or ArKO liver but had the highest level of MDR1 expression at both the mRNA and the protein levels. The in vivo results showed a lower retention of ^{64}Cu-ATSM and -PTSM in ArKO mice, despite a fatty liver indicating that although lipophilicity may favor initial penetration of the radiotracers, it is not sufficient to cause retention (*29*). Interestingly, ArKO liver retention and expression values were intermediate between wild-type and ArkO liver tumor,

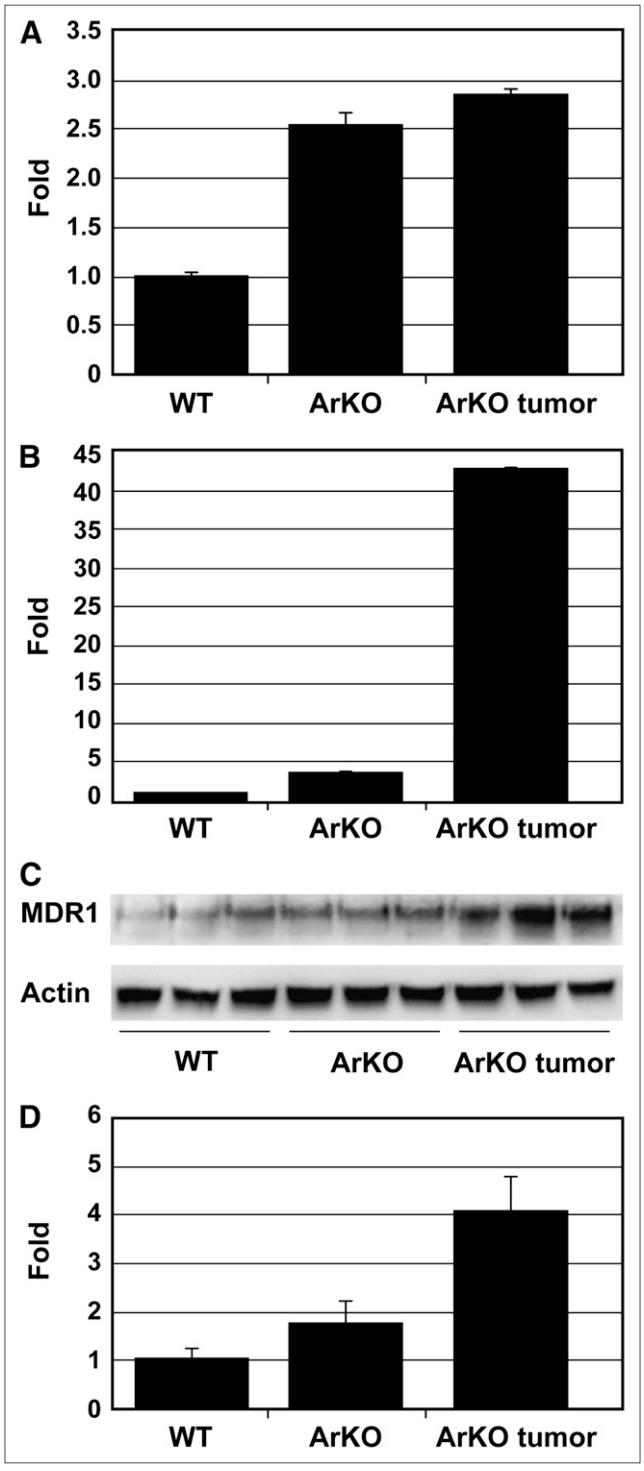

FIGURE 3. Mdr1a and Mdr1b expression is elevated in liver of ArKO mice and ArKO mice with liver tumor (A and B). Mdr1a and Mdr1b mRNA levels were quantified by qRT-PCR using glyceraldehyde-3-phosphate dehydrogenase as a reference gene. Wild-type liver had lowest levels of proteins, correlating with higher ^{64}Cu-ATSM retention. (C) Western blot analysis of Mdr1 protein expression. Anti-MDR1 antibody does not distinguish between Mdr1a and Mdr1b. Approximately 170-kD MDR1 band is highest in ArKO liver tumor. (D) Quantitative analysis of Western blot.

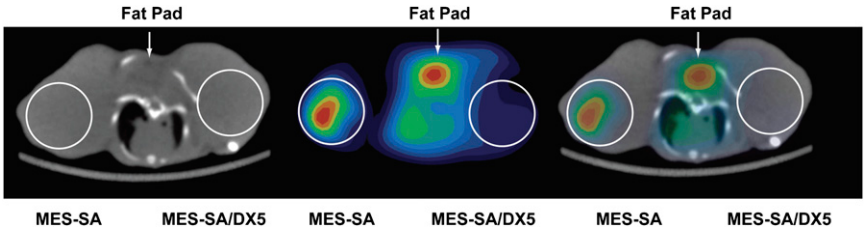

FIGURE 4. PET/CT shows decreased retention of ^{64}Cu-ATSM in MES-SA/Dx5 xenografts. One hour after intravenous injection of 3.7 MBq (100 μCi) of ^{64}Cu-ATSM, whole-body PET/CT images were acquired of mice bearing MES-SA xenografts about right shoulder and MES-SA/Dx5 xenografts on left. Axial sections are shown. MES-SA/Dx5 xenograft clearly shows less activity. Results are representative of studies on 3 different mice.

similar to the inverse relationship of ^{99m}Tc-MIBI retention and MDR1 expression that has been noted in several cancers (*5,6,10,30–33*). Whether such an inverse relationship exists with ^{64}Cu-ATSM and -PTSM retention is unknown but could be the subject of future clinical studies.

The in vivo studies were limited in that a causal relationship between elevated MDR1 expression and decreased retention of ^{64}Cu-PTSM and ^{64}Cu-ATSM could not be definitively established. Our in vitro cellular studies used MES-SA (MDR1−) and MES-SA/Dx5 (MDR1+) under ambient oxygen conditions, allowing us to study the influence of MDR1 independent of hypoxia or perfusion. MES-SA/Dx5 cells showed lower retention of either tracer in a time-dependent fashion and more rapid efflux. A strength of the in vitro studies was the use of RNA interference technology to specifically manipulate MDR1 expression. Using this approach, we could specifically show that MDR1 had a role in the retention of ^{64}Cu-ATSM and -PTSM. In the case of both radiotracers, knockdown of MDR1 protein resulted in an increase in cellular retention and a decrease in the efflux rate. Interestingly, the 70% knockdown of MDR1 expression was more effective in normalizing ^{64}Cu-ATSM than ^{64}Cu-PTSM retention. The reasons for the difference are unclear, but the finding suggests differences in how the cells handle the 2 radiotracers.

The mechanisms underlying ^{64}Cu-ATSM retention are incompletely understood. Two major mechanisms have been proposed. Initial cell penetration is facilitated by high lipophilicity. Fujibayashi et al. (*14*) first suggested that Cu(II)-ATSM reduction occurred only in hypoxic cells and was then irreversibly trapped. Obata et al. (*34*) presented evidence that reduction of ^{64}Cu-ATSM in normal cells (brain) occurred in mitochondria, whereas in tumors it occurred mainly in the microsome or cytosol fraction and involved the bioreductive enzymes NADH-cytochrome b5 reductase and NADPH-cytochrome P450 reductase. This enzymatic reduction was enhanced by hypoxia. Reports by Dearling et al. (*35*) and Maurer et al. (*36*) suggested that the reduction of Cu(II)-ATSM takes place in both normoxic and hypoxic cells, resulting in unstable Cu(I)-ATSM, which will slowly dissociate. Once the dissociation occurs it is irreversible and Cu(I) is trapped. In normoxic conditions Cu(I)-ATSM could be reoxidized and diffuse back out of the cell, but in hypoxic cells reoxidation is much less likely. Burgman et al. (*37*) suggested that Cu(I) is not irreversibly trapped but is absorbed into the intracellular copper pool, in which it becomes subject to cellular copper metabolism including efflux by copper exporters such as ATP7A/B. Whichever proposed model is correct, our results strongly suggest MDR1 affects the intracellular availability of Cu(II)-ATSM for the initial reduction or enhances efflux of Cu(I)-ATSM or Cu(II)-ATSM (namely reoxidized Cu(I)-ATSM) because it does not transport metals.

Several studies have shown tumor specificity in the hypoxia selectivity of ^{64}Cu-ATSM or correlation of ^{64}Cu-ATSM retention with modulation of tumor oxygenation, suggesting factors other than oxygen status may affect ^{64}Cu-ATSM retention (*17–19,37*). O'Donoghue et al. (*18*) found that intratumoral ^{64}Cu-ATSM distribution in human squamous cell xenografts agreed with oxygen microelectrode data at all times of the study, but prostate tumor xenografts showed agreement only at 16–20 h after injection. Burgman et al. (*37*), using multiple different rodent and human cell lines, found uptake and retention of ^{64}Cu-ATSM under different oxygenation conditions to be cell line–dependent. Yuan et al. (*19*) found that the autoradiographic distribution of ^{64}Cu-ATSM did not always agree with the distribution of the hypoxia probe EF5 on immunostaining. Carbogen breathing, which oxygenated the noncorrelative tumor, did not result in a decrease in ^{64}Cu-ATSM tumor uptake. Finally, Matsumoto et al. (*17*) studied ^{64}Cu-ATSM retention in squamous cell carcinoma cells in response to modulation of tumor oxygenation. These investigators were unable to demonstrate predictable changes in ^{64}Cu-ATSM tumor uptake when the tumor oxygenation status was varied before

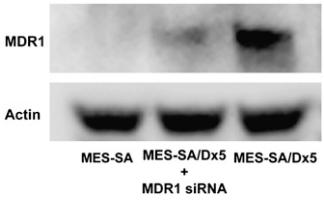

FIGURE 5. Knockdown of MDR1 by siRNA decreases protein levels. Protein extracts were prepared from control transfected–MES-SA/Dx5 cells or MDR1 siRNA–transfected cells 24 h after start of transfection. Relative levels of MDR1 protein were assessed by Western blotting. Data are representative of 3 independent experiments.

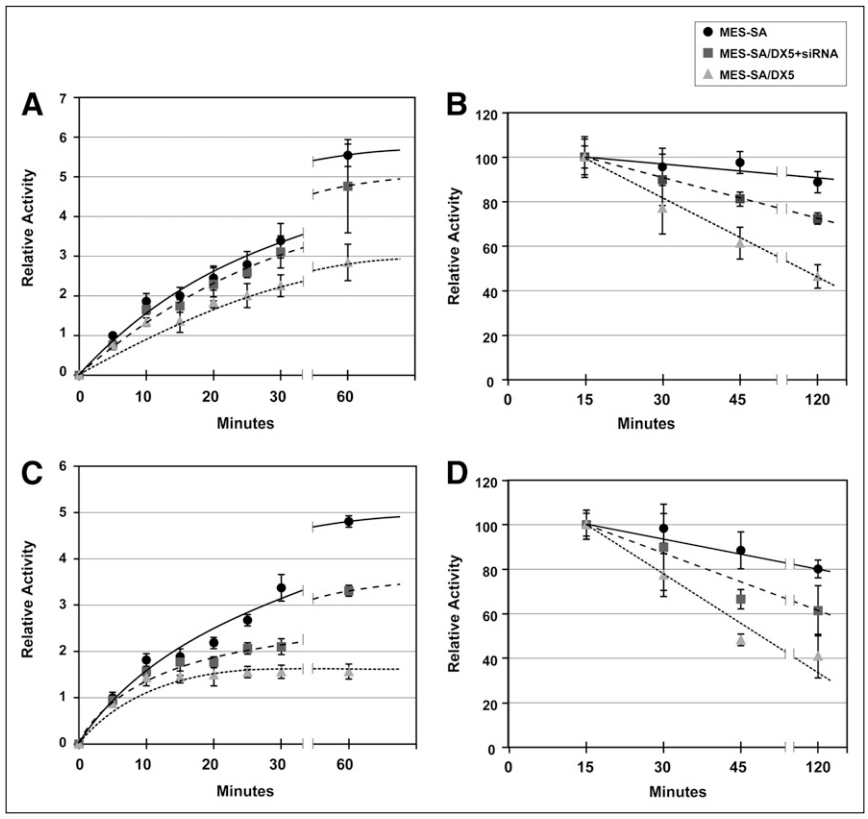

FIGURE 6. MES-SA/Dx5 cells retain lower levels of ^{64}Cu-ATSM/PTSM and show more rapid efflux; knockdown of MDR1 protein leads to increased retention and slower efflux. After transfection with control or MDR1 siRNA duplexes, cells were incubated with radiotracers for up to 1 h (A and C), and medium was removed. In efflux experiments, cells were loaded with radiotracer for 15 min. Medium was then replaced with cold medium, and incubation continued for times up to 2 h (B and D). Cells were quickly washed and lysed in buffered detergent solution. Activity in cell lysates was determined and expressed as counts per milligram of protein. (A and B) Uptake and efflux of ^{64}Cu-ATSM. (C and D) Uptake and efflux of ^{64}Cu-PTSM. Results are expressed as mean ± SEM. Data represent average of 3 independent experiments with triplicates in each group. Lines in graph were hand-drawn.

the uptake study. The investigators question the use of ^{64}Cu-ATSM as a hypoxia-specific marker and suggest that the avid binding of ^{64}Cu-ATSM to tumors may involve mechanisms independent of hypoxia that warrant further study. Together, all these studies show that tumor retention of ^{64}Cu-ATSM is complex and may not always reflect hypoxia but may depend on other tumor-specific factors. MDR1 expression or activity may be one such factor.

Two preclinical studies have been published using ^{64}Cu-ATSM radiotherapy (*38,39*). Lewis et al. (*38*) showed increased survival in ^{64}Cu-ATSM–treated hamsters bearing human colon cancer tumors. Aft et al. (*39*) found that when mice bearing mammary tumors were treated with ^{64}Cu-ATSM and 2-deoxyglucose, Cu-ATSM retention was increased, tumor growth slowed, and survival increased. Interestingly, 2-deoxyglucose depletes ATP, a necessary cofactor for normal MDR1 function. It is tempting to speculate that therapeutic results on humans could be enhanced with well-known MDR1 inhibitors, such as verapamil or in vivo siRNA when it becomes feasible.

CONCLUSION

The expression of MDR1 glycoprotein affects the retention of ^{64}Cu-ATSM and -PTSM in the human and murine tumors tested. These results may have implications on diagnostic clinical hypoxia imaging in tumors and the therapeutic efficacy of ^{64}Cu-ATSM. Prospective clinical studies on the relationship between MDR1 expression and ^{64}Cu-ATSM retention may be useful. Retrospective reviews of MDR1 expression in archived tumoral specimens with low ^{64}Cu-ATSM retention may help to demonstrate the clinical relevance of our findings.

ACKNOWLEDGMENTS

We thank Jeffery Ford for technical assistance, Michael Long for PET/CT imaging, and Glenn Katz for graphics support. This work was aided in part by unrestricted funds from the endowment of the Effie and Wofford Cain Distinguished Chair in Diagnostic Imaging, a graduate student scholarship awarded by the Scholarship Council of China through the State Scholarship Funds, and startup funds provided by the Department of Radiology and the Harold C. Simmons Comprehensive Cancer Center at UT Southwestern Medical Center at Dallas. ATSM and PTSM were kindly provided by Jason S. Lewis and Michael J. Welch of Washington University School of Medicine.

REFERENCES

1. Brown JM. The hypoxic cell: a target for selective cancer therapy—eighteenth Bruce F. Cain Memorial Award lecture. *Cancer Res.* 1999;59:5863–5870.
2. Gottesman MM, Fojo T, Bates SE. Multidrug resistance in cancer: role of ATP-dependent transporters. *Nat Rev Cancer.* 2002;2:48–58.
3. Endicott JA, Ling V. The biochemistry of P-glycoprotein-mediated multidrug resistance. *Annu Rev Biochem.* 1989;58:137–171.
4. Piwnica-Worms D, Chiu ML, Budding M, Kronauge JF, Kramer RA, Croop JM. Functional imaging of multidrug-resistant P-glycoprotein with an organotechnetium complex. *Cancer Res.* 1993;53:977–984.

5. Aratani T, Narabayashi I, Komori T, et al. Usefulness of Tc-99m MIBI SPECT in predicting multidrug resistance gene expression levels in non-small cell lung cancer: a preliminary report. *Ann Nucl Med.* 2001;15:313–319.
6. Burak Z, Moretti JL, Ersoy O, et al. ^{99m}Tc-MIBI imaging as a predictor of therapy response in osteosarcoma compared with multidrug resistance-associated protein and P-glycoprotein expression. *J Nucl Med.* 2003;44:1394–1401.
7. Cermik TF, Altiay G, Firat MF, Hatipoglu ON, Berkarda S. Assessment of Tc-99m sestamibi tumor tissue uptake under the influence of increased arterial oxygen saturation. *Nucl Med Biol.* 2005;32:165–170.
8. Kinuya S, Li XF, Yokoyama K, et al. Reduction of ^{99m}Tc-sestamibi and ^{99m}Tc-tetrofosmin uptake in MRP-expressing breast cancer cells under hypoxic conditions is independent of MRP function. *Eur J Nucl Med Mol Imaging.* 2003; 30:1529–1531.
9. Kinuya S, Yokoyama K, Li XF, et al. Hypoxia-induced alteration of tracer accumulation in cultured cancer cells and xenografts in mice: implications for pre-therapeutic prediction of treatment outcomes with ^{99m}Tc-sestamibi, ^{201}Tl chloride and ^{99m}Tc-HL91. *Eur J Nucl Med Mol Imaging.* 2002;29:1006–1011.
10. Zhou J, Higashi K, Ueda Y, et al. Expression of multidrug resistance protein and messenger RNA correlate with ^{99m}Tc-MIBI imaging in patients with lung cancer. *J Nucl Med.* 2001;42:1476–1483.
11. Lee ST, Scott AM. Hypoxia positron emission tomography imaging with ^{18}F-fluoromisonidazole. *Semin Nucl Med.* 2007;37:451–461.
12. Vavere AL, Lewis JS. Cu-ATSM: a radiopharmaceutical for the PET imaging of hypoxia. *Dalton Trans.* 2007;43:4893–4902.
13. Petering HG, Buskirk HH, Underwood GE. The anti-tumor activity of 2-keto-3-ethoxybutyraldehyde bis(thiosemicarbazone) and related compounds. *Cancer Res.* 1964;24:367–372.
14. Fujibayashi Y, Taniuchi H, Yonekura Y, Ohtani H, Konishi J, Yokoyama A. Copper-62-ATSM: a new hypoxia imaging agent with high membrane permeability and low redox potential. *J Nucl Med.* 1997;38:1155–1160.
15. Dehdashti F, Grigsby PW, Mintun MA, Lewis JS, Siegel BA, Welch MJ. Assessing tumor hypoxia in cervical cancer by positron emission tomography with ^{60}Cu-ATSM: relationship to therapeutic response—a preliminary report. *Int J Radiat Oncol Biol Phys.* 2003;55:1233–1238.
16. Dehdashti F, Mintun MA, Lewis JS, et al. In vivo assessment of tumor hypoxia in lung cancer with ^{60}Cu-ATSM. *Eur J Nucl Med Mol Imaging.* 2003;30:844–850.
17. Matsumoto K, Szajek L, Krishna MC, et al. The influence of tumor oxygenation on hypoxia imaging in murine squamous cell carcinoma using [^{64}Cu]Cu-ATSM or [^{18}F]fluoromisonidazole positron emission tomography. *Int J Oncol.* 2007; 30:873–881.
18. O'Donoghue JA, Zanzonico P, Pugachev A, et al. Assessment of regional tumor hypoxia using ^{18}F-fluoromisonidazole and ^{64}Cu(II)-diacetyl-bis(*N*4-methylthiosemicarbazone) positron emission tomography: comparative study featuring microPET imaging, PO_2 probe measurement, autoradiography, and fluorescent microscopy in the R3327-AT and FaDu rat tumor models. *Int J Radiat Oncol Biol Phys.* 2005;61:1493–1502.
19. Yuan H, Schroeder T, Bowsher JE, Hedlund LW, Wong T, Dewhirst MW. Intertumoral differences in hypoxia selectivity of the PET imaging agent ^{64}Cu(II)-diacetyl-bis(*N*4-methylthiosemicarbazone). *J Nucl Med.* 2006;47:989–998.
20. Harker WG, Sikic BI. Multidrug (pleiotropic) resistance in doxorubicin-selected variants of the human sarcoma cell line MES-SA. *Cancer Res.* 1985;45:4091–4096.
21. Fisher CR, Graves KH, Parlow AF, Simpson ER. Characterization of mice deficient in aromatase (ArKO) because of targeted disruption of the cyp19 gene. *Proc Natl Acad Sci USA.* 1998;95:6965–6970.
22. Fujibayashi Y, Yoshimi E, Waki A, et al. A novel ^{111}In-labeled antisense DNA probe with multi-chelating sites (MCS-probe) showing high specific radioactivity and labeling efficiency. *Nucl Med Biol.* 1999;26:17–21.
23. Young H, Carnochan P, Zweit J, Babich J, Cherry S, Ott R. Evaluation of copper(II)-pyruvaldehyde bis (*N*-4-methylthiosemicarbazone) for tissue blood flow measurement using a trapped tracer model. *Eur J Nucl Med.* 1994;21:336–341.
24. Hirasawa G, Simpson ER, Oz OK. Increased incidence of hepatic masses in aromatase deficient mice. Paper presented at: ENDO 2002, The Endocrine Society's 84th Annual Meeting; 2002; San Francisco, CA.
25. Rice GC, Ling V, Schimke RT. Frequencies of independent and simultaneous selection of Chinese hamster cells for methotrexate and doxorubicin (adriamycin) resistance. *Proc Natl Acad Sci USA.* 1987;84:9261–9264.
26. Liang BC. Effects of hypoxia on drug resistance phenotype and genotype in human glioma cell lines. *J Neurooncol.* 1996;29:149–155.
27. Luk CK, Veinot-Drebot L, Tjan E, Tannock IF. Effect of transient hypoxia on sensitivity to doxorubicin in human and murine cell lines. *J Natl Cancer Inst.* 1990;82:684–692.
28. Sakata K, Kwok TT, Murphy BJ, Laderoute KR, Gordon GR, Sutherland RM. Hypoxia-induced drug resistance: comparison to P-glycoprotein-associated drug resistance. *Br J Cancer.* 1991;64:809–814.
29. Jones ME, Thorburn AW, Britt KL, et al. Aromatase-deficient (ArKO) mice have a phenotype of increased adiposity. *Proc Natl Acad Sci USA.* 2000;97:12735–12740.
30. Ciarmiello A, Del Vecchio S, Silvestro P, et al. Tumor clearance of technetium 99m-sestamibi as a predictor of response to neoadjuvant chemotherapy for locally advanced breast cancer. *J Clin Oncol.* 1998;16:1677–1683.
31. Kunishio K, Okada M, Matsumoto Y, Nagao S, Nishiyama Y. Technetium-99m sestamibi single photon emission computed tomography findings correlated with P-glycoprotein expression in pituitary adenoma. *J Med Invest.* 2006;53:285–291.
32. Shih CM, Hsu WH, Huang WT, Wang JJ, Ho ST, Kao A. Usefulness of chest single photon emission computed tomography with technetium-99m methoxy-isobutylisonitrile to predict taxol based chemotherapy response in advanced non-small cell lung cancer. *Cancer Lett.* 2003;199:99–105.
33. Vecchio SD, Ciarmiello A, Potena MI, et al. In vivo detection of multidrug-resistant (MDR1) phenotype by technetium-99m sestamibi scan in untreated breast cancer patients. *Eur J Nucl Med.* 1997;24:150–159.
34. Obata A, Yoshimi E, Waki A, et al. Retention mechanism of hypoxia selective nuclear imaging/radiotherapeutic agent cu-diacetyl-bis(*N*4-methylthiosemicarbazone) (Cu-ATSM) in tumor cells. *Ann Nucl Med.* 2001;15:499–504.
35. Dearling JL, Lewis JS, Mullen GE, Welch MJ, Blower PJ. Copper bis(thiosemicarbazone) complexes as hypoxia imaging agents: structure-activity relationships. *J Biol Inorg Chem.* 2002;7:249–259.
36. Maurer RI, Blower PJ, Dilworth JR, Reynolds CA, Zheng Y, Mullen GE. Studies on the mechanism of hypoxic selectivity in copper bis(thiosemicarbazone) radiopharmaceuticals. *J Med Chem.* 2002;45:1420–1431.
37. Burgman P, O'Donoghue JA, Lewis JS, Welch MJ, Humm JL, Ling CC. Cell line-dependent differences in uptake and retention of the hypoxia-selective nuclear imaging agent Cu-ATSM. *Nucl Med Biol.* 2005;32:623–630.
38. Lewis J, Laforest R, Buettner T, et al. Copper-64-diacetyl-bis(*N*4-methylthiosemicarbazone): an agent for radiotherapy. *Proc Natl Acad Sci USA.* 2001;98:1206–1211.
39. Aft RL, Lewis JS, Zhang F, Kim J, Welch MJ. Enhancing targeted radiotherapy by copper(II)diacetyl-bis(*N*4-methylthiosemicarbazone) using 2-deoxy-D-glucose. *Cancer Res.* 2003;63:5496–5504.

JNM The Journal of NUCLEAR MEDICINE

Retention of the Radiotracers ^{64}Cu-ATSM and ^{64}Cu-PTSM in Human and Murine Tumors Is Influenced by MDR1 Protein Expression

Jun Liu, Asghar Hajibeigi, Gang Ren, Mai Lin, Wasana Siyambalapitiyage, Zhisu Liu, Evan Simpson, Robert W. Parkey, Xiankai Sun and Orhan K. Öz

J Nucl Med. 2009;50:1332-1339.
Published online: July 17, 2009.
Doi: 10.2967/jnumed.109.061879

The Journal of Nuclear Medicine is published monthly.
SNMMI | Society of Nuclear Medicine and Molecular Imaging
1850 Samuel Morse Drive, Reston, VA 20190.
(Print ISSN: 0161-5505, Online ISSN: 2159-662X)

SNMMI SOCIETY OF NUCLEAR MEDICINE AND MOLECULAR IMAGING